JCTC Journal of Chemical Theory and Computation

Comparative Static and Dynamic Study of a Prototype S_N2 Reaction

Laurent Joubert,[†] Michele Pavone,[‡] Vincenzo Barone,[‡] and Carlo Adamo*[,†]

Laboratoire d'Electrochimie et de Chimie Analytique, UMR CNRS 7575, Ecole Nationale Supérieure de Chimie de Paris, 11, rue Pierre et Marie Curie, 75231 Paris Cedex 05, France, and Laboratorio di Struttura e Dinamica Molecolare, Dipartimento di Chimica, Complesso Universitario Monte Sant'Angelo, Via Cintia, I-80126 Napoli, Italy

Received January 10, 2006

Abstract: Ab initio molecular-dynamic simulations, using density functional theory (DFT) and the recent atom-centered density-matrix propagation method (ADMP), were used to study the bond formation process in a prototypical S_N2 reaction, namely the Walden inversion. Using the real space partition schemes of both electronic density and electron localization function gradient fields, we analyzed different quantum chemical topology (QCT) properties along the ADMP trajectory. In particular, atomic charges derived from the Bader's atoms-in-molecules (AIM) theory were used to analyze intra- and intermolecular charge transfers between atoms, while the electronic population of the forming bonding basin obtained from the electron localization function (ELF) gradient field was employed to describe the bond formation process. These results were compared to the corresponding QCT properties issuing from a static approach based on the intrinsic reaction path (IRP). Although similar features are found for both static and dynamic approaches, the dynamic QCT analysis provides some explanation of the differences observed during the formation of the ion−molecule complex. In particular, it suggests a stronger electron exchange leading to an effective maximization of both covalent and noncovalent interactions.

1. Introduction

The interpretation of the numerical results issuing from quantum chemical calculations in terms of classical chemical concepts is not a straightforward task. For instance, electron transfer is strongly related to the definition of atoms and bonds in a molecular system. Beyond the basic picture of Lewis[1] based on intuitive concepts, at least two different models have been proposed with the aim of obtaining quantitative information on the nature of chemical bond. On one hand, classical localization procedures of the one-electron density matrix and/or overlap matrix lead to different definitions of atomic charges (e.g. Mulliken or Löwdin ones[2,3]) or to hybrid orbitals (see for instance refs 4−6). On the other hand, quantum chemical topological (QCT) analyses based on the electronic density, i.e., the Bader's atoms in molecules (AIM) partition scheme[7,8] or on derived functions, such as the electron localization function (ELF),[9−11] have convincingly shown their reliability and robustness. In particular, these methods are well suited to characterize chemical bonds[12−15] or to get insights into the reactivity of molecular systems.[7,8,16−20]

Nowadays, a wide choice of tools is available to chemists for the theoretical analysis of different classes of chemical reactions. These tools are even more powerful when coupled with efficient algorithms for the exploration of potential energy surfaces (PES), such as those based on the intrinsic reaction coordinate (IRC) concept.[21] Calculation of topological or electronic variables along the reaction path provides a clear-cut picture of the reaction mechanism and for rationalizing the structural/energetic properties of the stationary points on the PES (reactants, transition states, and products).[22,23] It must be pointed out, however, that all these approaches have been developed in the framework of a time-

* Corresponding author e-mail: carlo-adamo@enscp.fr.
[†] Ecole Nationale Supérieure de Chimie de Paris.
[‡] Complesso Universitario Monte Sant'Angelo.

10.1021/ct0600159 CCC: $33.50
Published on Web 08/04/2006

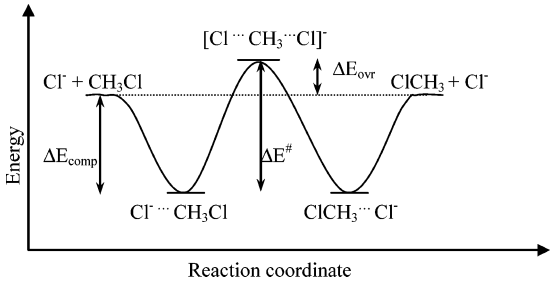

Figure 1. Sketch of energy profile for the S_N2 reaction under study.

independent (i.e. static) view. Only recently Gross and co-workers have formulated a suitable but rather complex approach introducing a time dependent ELF.[24]

At the same time, methods rooted on the so-called ab initio molecular dynamics, both in Born−Oppenheimer and extended Lagrangian versions, are today well assessed and have been widely used for reactivity studies.[25−27] In particular, the so-called Car−Parrinello approach,[28] using an extended Lagrangian scheme, is based on the evaluation of energies and gradients at the density functional theory level (DFT) and on the contemporary propagation of electronic and nuclear degrees of freedom.[29] The time evolution of any property is then easily computed a posteriori from suitable statistical averages of single point evaluations on snapshots extracted from the trajectory.[29]

An attempt to explore the difference between static and dynamic ab initio approaches has been performed,[30] but it has been focused mainly on the thermochemistry, since the choice of unique and meaningful parameters for comparison is not trivial.

In the present article, we report a study concerning the complex charge-transfer processes driving the bond breaking and formation processes in a prototype reaction. The static approach is based on the standard IRC model, while the dynamic one rests on an extended Lagrangian approach employing atom-centered (Gaussian) functions, the so-called atom-centered density matrix propagation (ADMP) model.[31] Our aim is to elucidate the differences, and the common aspects, between both approaches in the analysis of bond breaking/formation. To this end, we have chosen topological quantities as probe molecular descriptors. The so-called Walden inversion, the S_N2 reaction sketched in Figure 1, has been chosen as a model, since it is a simple and well-studied reaction, from both a static and dynamical point of view.[32−52] In the present study we limit our analysis to the gas-phase reaction, and we do not consider solvent effects which are known to strongly modify the potential energy surface (PES).[35]

2. Computational Details

All the calculations were carried out with the Gaussian 03 program,[53] using the hybrid PBE0 functional[36,54] and the 6-31+G(d,p) basis set.[55] Starting from the transition state, we calculated reaction pathways by both static and dynamic approaches. On one hand, we followed the intrinsic reaction path (IRP) between the transition state and the stable ion−molecule complex.[21] On the other hand, the dynamic simulation was performed at 298 K in the canonical ensemble, for a total simulation time of 1.5 ps. The starting point (transition state) was previously optimized with the same basis set and functional used in the simulation. The velocity-Verlet algorithm[56] was employed for the integration of the equations of motions using a time step of 0.25 fs. The fictitious mass of the electron was set to 0.20 amu with a scaling both for core and valence electrons as described in ref 31. The velocities of the nuclei were scaled each five time steps to ensure a constant temperature within a $\Delta T = 5$ K tolerance. The stability of the simulations was monitored by checking at each step the idempotency of the density matrix (within a 10^{-12} threshold) and the so-called adiabaticity index (within a 10^{-4} threshold, see ref 31 for more details). In practice, we restricted our trajectory investigation to the time frame of interest, analyzing the path only during the formation of the stable ion−molecule complex. Along this truncated trajectory (shorter than 100 fs in time scale), we extracted a number of snapshots, spaced by 2 fs, for the subsequent structural and electronic analyses of the reaction.

The charge-transfer processes were investigated using a QCT approach, namely the AIM partition scheme of the electronic density.[7,8] According to this model, a topological atom is defined as a region of the real space consisting of a bundle of electron density gradient paths attracted by a nucleus. This partition allows evaluating atomic properties, defined as volume integrals over nonoverlapping atomic basins. In particular, the electron population associated with an atom is simply the volume integral of the electronic charge density over the basin. Other useful properties can be derived such as the delocalization index, providing a quantitative measure of the sharing of electrons between two atomic basins.[13]

Another partition of the electronic density can be achieved by considering the electron localization function ($\eta(\mathbf{r})$, ELF)[9] which can be viewed, to a good approximation, as a compact form of the spin-pair composition function, relying on a chemical approach to describe the nature of the electron cloud in terms of parallel and antiparallel spin-pair concentrations.[57] In practice, portions of the real space characterized by a high probability to find antiparallel spin-pair concentrations correspond to values of $\eta(\mathbf{r})$ close to 1. In contrast, other portions where the probability to find parallel spin-pair concentrations is low are characterized by $\eta(\mathbf{r})$ values close to 0. During the 1990s, Silvi and co-workers proposed a gradient field topological analysis of this bounded function,[10,11] providing a quantum chemical reformulation of the empirical Lewis chemical bond model. The topology of this gradient field is more complex than the one of the electronic density, presenting nonatomic basins such as bonding basins, shared between two or more neighboring atoms (see ref 11 for details on the nature of these basins). The electronic population of these basins can be viewed as a quantitative measure of bond strengths in terms of covalence, i.e., the sharing of strongly localized, antiparallel spin pairs. As already mentioned in the Introduction, this "bonding" electronic population will be used in the following to describe the formation of the carbon−chlorine covalent bond, as a complement to AIM calculations. All QCT calculations (AIM

Table 1. Computed Main Geometry Parameters (Å) for the Equilibrium Ion−Dipole Complex and the Transition State

	complex		transition state
	$d(C-Cl_1)$	$d(C-Cl_2)$	$d(C-Cl)$
MP2/TZ3P+R+(2f,d)[a]	3.27	1.81	2.32
CCSD(T)/TZ+2Pf+dif[b]	3.15	1.82	2.30
BP/TZ+2P[b]	3.10	1.84	2.34
OLYP/TZ+2P[c]	3.37	1.83	2.36
mPW1PW/6-31+G(d,p)[d]	3.01	1.83	2.33
PBE0/6-31+G(d,p)	3.16	1.82	2.33
PBE0/6-311++G(3df,2dp)	3.14	1.81	2.31

[a] Reference 37. [b] Reference 45. [c] Reference 46. [d] Reference 35.

and ELF) have been performed with the Topmod package[58] and local scripts.

3. Results

Before discussing in some detail the results of our analysis, we want to add some general remarks on the topological approaches chosen. Recently, Chevreau and co-workers[59] have combined AIM calculations with dynamic simulations to explore charge-spin transfers in model molecules introducing what they refer to as time-dependent topological analyses. In contrast, we prefer to follow the proposition of Popelier[8] and use the more specific definition of quantum chemical topology (QCT). The main point is that QCT embraces both AIM and ELF topological analyses and any approaches that adopt the topological idea.[60] Therefore, we will refer in the following to dynamic quantum chemical topology (DQCT) for QCT analyses performed in the framework of a dynamic treatment of the reactivity, since time is not an explicit variable neither for the property nor for the electron density. Similarly, a QCT study realized along an intrinsic reaction path, i.e., a static approach of the reactivity, will be referred to as a static quantum chemical topology (SQCT) analysis.

3.1. Tuning the DFT Approach. The prototypical S_N2 reaction studied in the present work (see Figure 1) is characterized in the gas phase by a double-well potential energy surface with two equivalent local minima corresponding to the formation of a pre- and a postreaction ion−molecule complex ($Cl^-\cdots CH_3Cl$) and a transition state (TS) of D_{3h} symmetry ($[Cl\cdots CH_3\cdots Cl]^-$). Due to the overall symmetry of the reaction, we will limit our study to a reaction path from the transition state to one of the equivalent minima.

We have chosen the PBE0 functional, which provides reliable thermodynamic data for the S_N2 reaction under study, when coupled to extended basis sets (e.g. 6-311+(3df,3pd)). Since a large number of calculations are needed in order to evaluate the variations of all the topological quantities along the trajectories, use of extended basis sets becomes prohibitive. For this reason, we performed some preliminary tests to assess the validity of the chosen functional with the medium size 6-31+G(d,p) basis set. We first examined the geometrical features of the key structures, i.e., the geometries of the ion−molecule complex and of the transition state. Structural and energetic results are summarized in Tables 1 and 2, respectively. From a structural point of view, our data are very close to MP2 results[38] for the transition state structure, with a deviation of about 0.01 Å for the carbon−chlorine distance. The same trends are observed for the $C-Cl_2$ bonding distance in the ion−molecule complex. In contrast, a larger error (0.20 Å) is observed for the $C\cdots Cl_1$ distance, this effect being related to basis set incompleteness. In fact, when the larger 6-311+G(2d,p) basis set is considered this distance increases significantly (3.23 Å), toward the MP2 value.

Table 2. Complexation Energies, Overall Energies, and Barrier Heights (in kcal/mol) for the Studied S_N2 Reaction

	ΔE_{comp}	ΔE_{ovr}	$\Delta E^{\#}$
MP2[a]/TZ3P+R+(2f,d); ZPE corrected	−10.5	3.5	14.0
MP4[b]TZ+2P; ZPE corrected	−10.6	1.8	12.4
G3;[c] ZPE corrected	−11.2	1.8	13.0
CBS-QB3(+);[c] ZPE corrected	−10.7	2.4	13.1
best ab initio results[d]	−11.3	1.6	12.9
BP/TZ+2P;[b] ZPE corrected	−10.3	−5.7	4.6
OLYP/TZ+2P;[e] ZPE corrected	−9.0	−0.1	8.9
B3LYP/6-31G(d);[f] ZPE corrected	−9.5	−0.9	8.7
mPW1PW/6-31+G(d,p);[g] ZPE corrected	−9.8	0.7	10.5
PBE0/6-31+G(d,p); ZPE corrected	−10.1	0.5	10.6
experiment[h]	−12 ± 2	3/1 ± 1	13 ± 2

[a] Reference 37. [b] Reference 38. [c] Reference 39. [d] Reference 45. [e] Reference 46. [g] Reference 35. [h] Reference 51.

The most significant thermodynamic quantities are the complexation energy of the ion−molecule species (ΔE_{comp}), the activation energy, i.e. the relative energy of the D_{3h} saddle point with respect to the ion−molecule complex ($\Delta E^{\#}$), and the overall barrier (ΔE_{ovr}), defined as the difference between ΔE_{comp} and $\Delta E^{\#}$. These data are reported in Table 2 and compared with selected previous theoretical and experimental results. While the computation of initial closed-shell reagents does not involve particular difficulties, the determination of the charged transition state energy $[Cl\cdots CH_3\cdots Cl]^-$ by DFT approaches is more involved. As a matter of fact, most of the standard functionals, and in particular those resting on the GGA, fail in determining the energy barriers. This effect has been related to the self-interaction error both in the exchange and in the correlation parts, which implies a too large delocalization of the electron density with the consequent overstabilization of the transition state (for a recent discussion about this point see ref 61). In contrast, PBE0 calculations provide accurate results, close to the best post-HF methods and well in the range of the experimental estimates. Of course, we cannot exclude that this result is due to a fortuitous error compensation between the GGA and HF contributions.

3.2. Static and Dynamic Topological Analyses. The energy variations along the IRP and the ADMP trajectory are reported in Figures 2 and 3, respectively. We recall that the IRP corresponds to a unique and constrained minimum energy path and does not contain any dynamic information, whereas the ADMP profile is computed along a trajectory issuing from a dynamic simulation. Therefore any straight (i.e. point-to-point) comparison can be misleading, but we think that global differences remain meaningful.

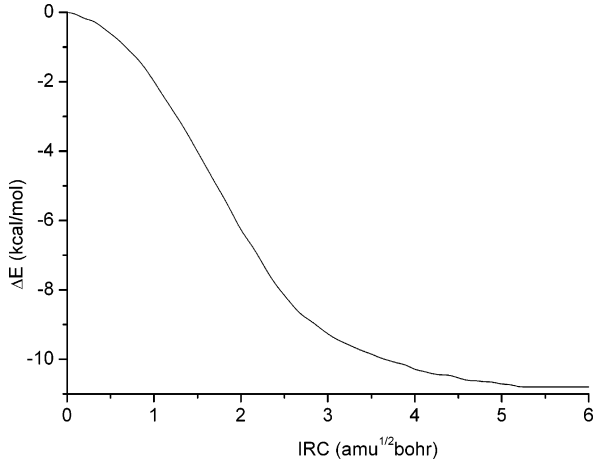

Figure 2. Plot of the potential energy profile along the IRP from the transition state to the ion−molecule complex.

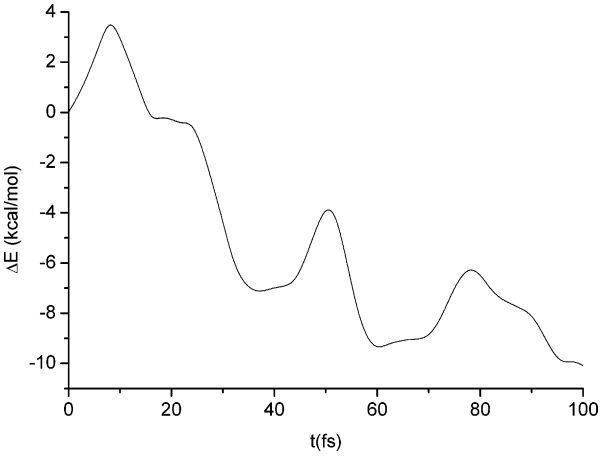

Figure 3. Plot of the potential energy profile along the ADMP trajectory from the transition state to the ion−molecule complex.

Table 3. Computed AIM Basin Populations (e^-) for the Transition State and the Ion−Molecule Complex

atom	transition state	ion−molecule complex	atom	transition state	ion−molecule complex
Cl1	17.70	17.95	H3	0.83	0.86
H1	0.83	0.84	C	6.11	6.10
H2	0.83	0.88	Cl2	17.70	17.38

The minimum energy constraint determines a unique IRP, on which the energy continuously decreases from the transition state to the minimum. In contrast, the energy globally decreases along the ADMP trajectory, but it appears clearly that the reaction does not follow this minimum energy path. Actually, the minimum is rapidly reached after 96 fs, but the curve exhibits some energy risings corresponding to local destabilizations of the whole system.

To rationalize the differences observed between static and dynamic approaches, we investigated the intra- and intermolecular charge transfers along the different reaction paths. As a first step, we analyzed the AIM atomic populations for the two states of interest, i.e., the transition state and ion−molecule complex. The results are collected in Table 3. At the transition state, each chlorine atom bears a negative

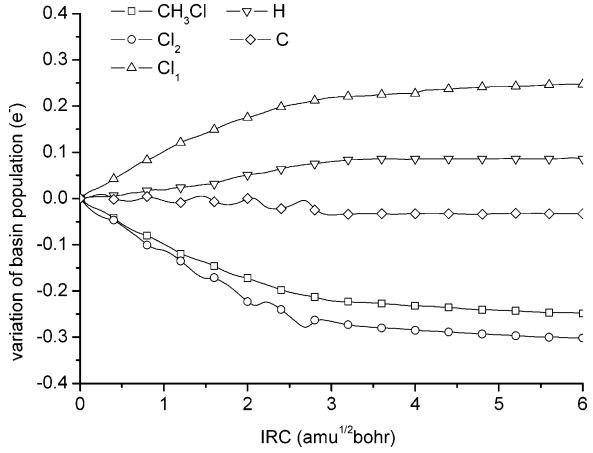

Figure 4. Variations of AIM populations along the IRP. The "superbasin" corresponding to the forming chloromethane molecule (5 basins) is represented by the solid curve.

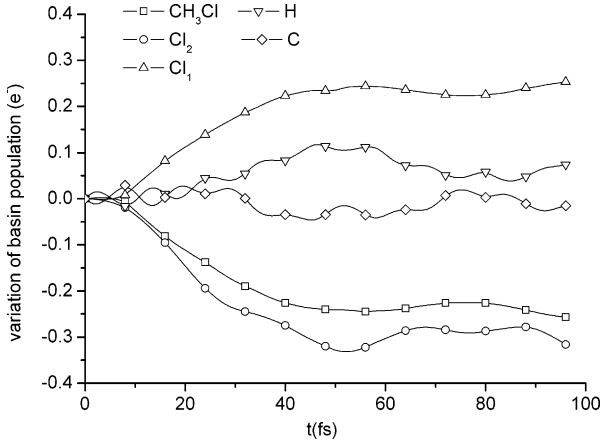

Figure 5. Variations of AIM populations along the ADMP trajectory. The "superbasin" corresponding to the forming chloromethane molecule (5 basins) is represented by the solid curve.

charge of −0.70 $|e^-|$. This electron excess corresponds to the sharing of the unit charge of the complex increased by a supplementary electron transfer of approximately 0.20 e^- from hydrogen atoms to each of the chlorine atom. Along the IRP, the formation of the ion−dipole molecule corresponds to a global charge transfer of 0.25 e^- from the incoming chloromethane moiety to the leaving chlorine atom. This charge transfer is slightly increased (by 0.01 e^-) when considering the dynamic process. This global molecule−ion interaction is accompanied by an intramolecular charge transfer in the forming chloromethane molecule. This phenomenon is evidenced by a slight increase of the electron population on the methyl moiety (0.05 and 0.06 e^- at the end of the static and dynamic process, respectively).

A deeper insight into the charge-transfers processes can be gained by examining the variations of the atomic electronic populations along the IRP and ADMP trajectory. Figures 4 and 5 show the relative variations of selected AIM basin populations with respect to the initial populations in the transition state configuration for the static and dynamic approach, respectively. We first examine the global mechanism, i.e., the molecule-to-ion charge transfer, evidenced

by two essential curves. The first one corresponds to the monotonically increasing atomic population of the leaving chlorine atom Cl1, tending to the population of an isolated chloride anion. In parallel, the second curve, grouping the atomic populations of the whole CH_3Cl molecule, shows the corresponding and decreasing electronic population of the forming molecule. When the ion−dipole complex is formed, the global electronic transfer between the two moieties corresponds to the aforementioned net charge of 0.25 $|e^-|$. Three additional curves are presented on the same graphs, corresponding to the variations of the atomic populations of (i) the chlorine atom Cl1 of the forming chloromethane molecule, (ii) the three hydrogen atoms taken together, and (iii) the carbon atom. If we examine these variations, substantial differences are observed between static and dynamic approaches.

A careful examination of the atomic population variations along the static IRP (Figure 4) allows us to propose a three-step charge-transfer mechanism. In the first part of the path, with a length of about 1.0 $amu^{1/2}$ Bohr, the electron excess on the Cl2 atom is transferred almost totally to the other chlorine through the atomic basins of the hydrogen atoms. This particular point is evidenced by examining the variations of the atomic populations of the two chlorine atoms that almost compensate each other. In other words, the electronic flux coming from the Cl2 basin and entering the three hydrogen basins corresponds to the exiting flux that penetrates the Cl1 basin. Besides this main electron transfer, a second one is observed between the carbon and the three hydrogen atoms. In fact, along the path, the carbon−hydrogen bond lengths systematically increase when the methyl group adopts a C_{3v} geometry in the forming molecule and points toward the leaving chlorine atom. This phenomenon is enhanced by an increasing favorable electrostatic interaction with this chlorine atom. Therefore, the lengthening of these bonds explains the local charge transfer observed from carbon to hydrogen atoms. Finally, we note substantial fluctuations in the population variations of the linked carbon and chlorine atoms, which, once again, compensate each other. In more detail, a small fraction of the electron flux between chlorine atoms penetrates the carbon basin, resulting in a small increase of the corresponding population that tends to be slightly in excess, whereas, at the same time, the formation of the carbon−chlorine bond counteracts this flux by inducing a small charge transfer from the carbon to the chlorine atom. In the second step of the charge-transfer mechanism, i.e., up to 3.0 $amu^{1/2}$ Bohr, the electron loss of the Cl2 atom becomes stronger than the electron gain of the leaving Cl1 atom. Therefore, the electron flux that enters the hydrogen basins becomes larger than the exiting flux with a consequent increase of the electron population in the hydrogen basins. The electron charge transfer from carbon to hydrogen atoms increases as well, though to a lower extent, thus reinforcing the electronic population of these basins. Furthermore, we note that the fluctuations observed along the carbon and chlorine (Cl2) curves are amplified when approaching the equilibrium structure of the chloromethane. The last step of the charge-transfer mechanism corresponds approximately to the second half of the IRP. Negligible structural changes are observed in the chloromethane molecule, resulting in equilibrium for carbon and hydrogen basin populations. The Cl1 atom continues to move away from the molecule leading to a strong decrease of the chlorine-to-chlorine charge transfer, the population of the Cl1 atom approaching that of a chloride anion.

The DQCT analysis of atomic population variations along the ADMP trajectory (see Figure 5) suggests a charge-transfer mechanism quite different from that issuing from the SQCT calculations. We can decompose it in five steps. We first note that the system is destabilized during the first 8 fs of the simulation (see Figure 2), certainly due to an excess of initial kinetic energy. During that period, population variations are negligible, except for the periodic fluctuations of the carbon and hydrogen populations corresponding to the C−H stretching mode. These fluctuations are present along the whole trajectory. The second dynamic step, occurring between 8 and 16 fs, is very similar to the first part of the IRC path, where an electron excess on the Cl2 atom is transferred almost totally to the other chlorine through the atomic basins of the hydrogen atoms. The third step corresponds roughly to time steps between 16 and 30 fs and can be compared to the second step of the IRC charge-transfer mechanism. In fact, the curve corresponding to the population variations of the Cl2 chlorine atom strongly deviates from the one corresponding to the population variations of the whole chloromethane molecule. Meanwhile, both electronic populations of carbon and hydrogen atoms substantially increase, indicating an intramolecular charge transfer from the Cl2 basin to the carbon and hydrogen basins. In contrast with the static approach, no fluctuations are observed for the carbon and Cl2 chlorine curves but for the periodic variations on the carbon curve corresponding to the C−H stretching vibration mode.

At this point, we want to remark that all the results discussed above are preserved when different initial conditions (kinetic energy and temperature) are considered, since the excess energy mainly affects the population of the CH vibrational states. This is not surprising since the $Cl-CH_3$-Cl starting ion-complex exhibits a rather poor energy transfer between the inter- and intramolecular vibrational modes.[42,62]

The third step corresponds to time frames between 30 and 50 fs. We observe that the electronic population of the hydrogen basins strongly increases due to a substantial electron transfer from the carbon basin. Moreover, the corresponding population variations almost compensate to each other. All these subtle variations are related to structural changes during the dynamics. On Figure 6, we isolated the population variations of the carbon and hydrogen basins together with the variations of C−H distances. During the time frame of interest, we note a substantial lengthening of these distances. This phenomenon was also observed along the static IRP but with smaller amplitude. Here, the C−H stretching mode increases the corresponding bond lengths, strengthening the electrostatic attraction between the leaving chlorine atom and hydrogen atoms and favoring the electron flux between them. This noncovalent effect should favor the stabilization of the system, but we know that the complex is strongly destabilized within this time frame, as evidenced

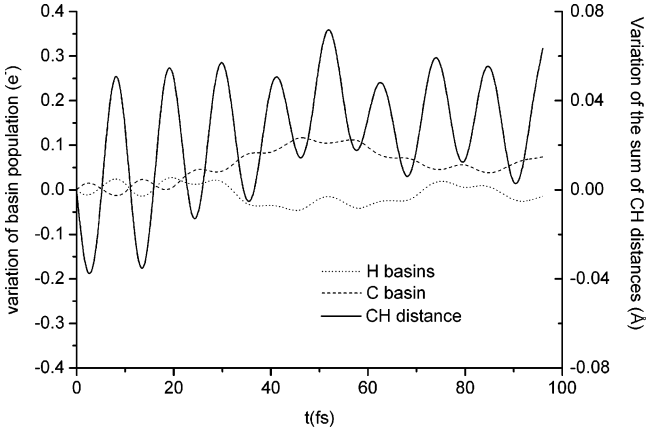

Figure 6. Comparison between the variations of selected basin populations (C and H) and the sum of C−H distances (solid line) along a dynamic pathway from the transition state to the ion−molecule complex.

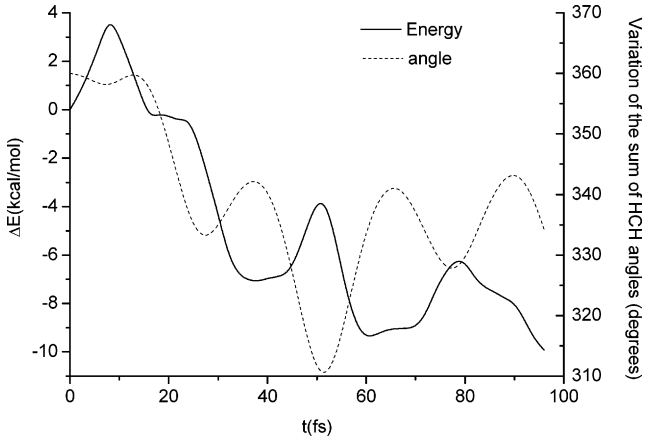

Figure 7. Comparison between the potential energy variations (in bold) and H−C−H valence angles (dash) along a dynamic pathway from the transition state to the ion−molecule complex.

by a sudden potential energy rising in Figure 3. This surprising behavior can be better rationalized by examining the structural evolution of the system. Figure 7 shows the variations of the potential energy together with the evolution of the H−C−H valence angles, i.e., we plotted the variations of the sum of these three angles along the trajectory. In the time interval of interest, we can see that the sum of angles reaches a minimum value (about 310°). In other words, the strong electrostatic attraction between the Cl1 chlorine atom and hydrogen atoms induces not only an increase of the C−H bond lengths but also a substantial narrowing of the H−C−H valence angles. The latter effect may explain at least partly the destabilization of the system by increasing electrostatic and Pauli repulsions between the hydrogen atoms. A deeper insight on this unexpected and sudden potential energy rising can be obtained from a topological description of the forming C−Cl2 bond. Even if AIM is, in our opinion, adequate for such a description,[14] Cioslowski and co-workers[63−65] and Feinberg and Ruedenberg[66] pointed out some problems inherent to the definition of a bond path in AIM. In this paper, we follow an alternative route offered by the DQCT analysis of the ELF gradient field. We choose here to focus

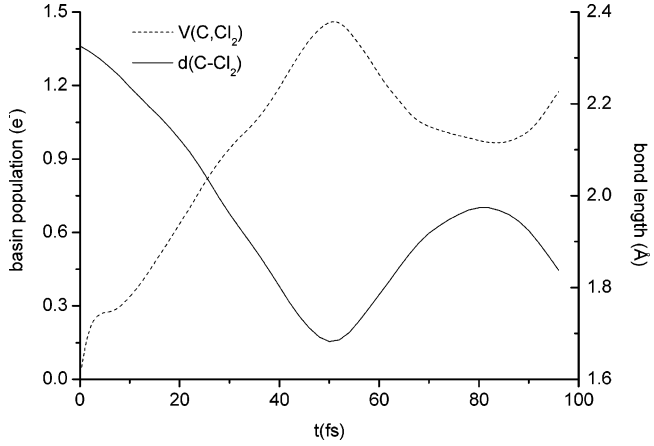

Figure 8. Left *Y* axis: variation of the C−Cl2 distance (in bold) along the ADMP trajectory. Right *Y* axis: variations of the forming bonding basin (C,Cl2) electronic population (dashed).

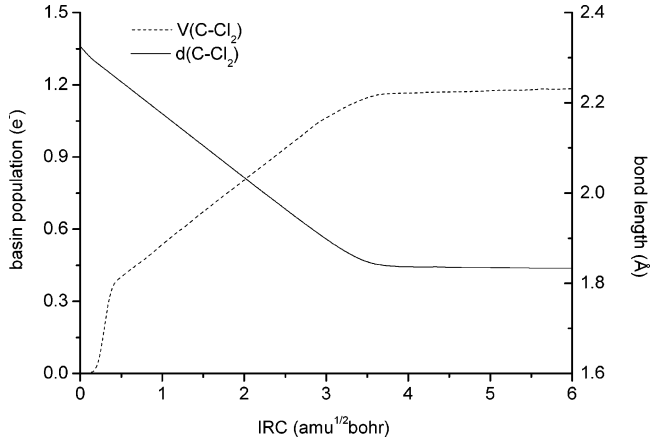

Figure 9. Left *Y* axis: variation of the C−Cl2 distance (in bold) along the IRP. Right *Y* axis: variations of the forming bonding basin (C,Cl2) electronic population (dashed).

on the forming bonding basin between the carbon and the incoming chlorine atom (Cl2). The variations of both the C−Cl2 bond distance and the electronic population of the corresponding bonding basin are represented in Figure 8. In the time interval corresponding to the second peak of energy increase, a continuous decrease of the C−Cl2 distance is observed, down to a global minimum value of 1.682 Å at $t = 50$ fs. This bond distance is about 0.15 Å shorter than the equilibrium value. Meanwhile, the electron population of the bonding basin dramatically increases up to reach a final value of 1.45 e^-, emphasizing a strong covalent character which is quite unexpected for such highly polarized interaction. In short, the electron sharing between carbon and chlorine is maximized during the dynamic simulation, leading to a very short interatomic distance and to the consequent destabilization of the whole system by a strong increase of the Pauli repulsion between atoms. It is noteworthy that a SQCT analysis (see Figure 9) does not exhibit such patterns, but, rather, points out a continuous decrease of the C−Cl2 bonding distance, corresponding to a normal increase of the bonding electronic population reaching an equilibrium value of 1.18e^-. Finally, the two last steps of the dynamic charge-

transfer mechanism correspond to the second half of the trajectory. First, between 50 and 78 fs, the system, strongly destabilized, tends to reduce quickly its potential energy. Thus, we note a sudden lengthening of the C−Cl2 bond and an opening of the H−C−H valence angles (see Figure 7) coupled with a shortening of the C−H bond lengths (see Figure 6). This last effect induces a strong lowering of the charge density transferred from the carbon to the hydrogen atoms. Moreover, it is important to point out an inverted electron flux from the ion to the chloromethane molecule, which tries to equilibrate the destabilized system. Finally, the last part of the dynamic trajectory, beyond 78 fs, corresponds to the effective formation of a stable ion−molecule complex and to the end of the charge transfer between the molecule and the chlorine atom stabilized by the completion of its external valence shell.

4. Some Comments on the Static vs Dynamic Descriptions

Our results show how both DQCT and SQCT approaches suggest that the driving force for the formation of the ion−molecule complex are the local charge-transfer processes. These processes lead to an increase and maximization of the number of electron pairs exchanged between atoms during the bond formation process. This picture is consistent with previous analyses, based on different theoretical models. Among others, we want to recall that similar even if much more qualitative conclusions were drawn several years ago by Shaik on the basis of arguments resting on valence bond (VB) calculations.[67] In the same philosophy, but more recently, it is has been suggested that, within a VB approach, the overlap between the active orbitals of the incoming Cl^- and CH_3Cl moieties rules the overall reactive process.[62] Moreover, the maximization of electron pairs sharing between atoms strongly reminds one of the "maximum localization hybrid orbitals" overlap principle suggested more than 30 years ago by Del Re.[68] This criterion has been used as a driving force in a chemical reactivity study based on semiempirical qualitative approaches.[69] Analogous results were also reached by Toro-Labbé using the principle of maximum hardness.[70]

Beyond the static approach of reactivity, we observe that this force is so enhanced in the dynamics simulation that it allows an overgrowing electronic population in the bonding basin, as evidenced by the QCT of the ELF function. This results in a very short C−Cl2 distance and in high energy. The subsequent increase of the Pauli repulsion is permitted to eventually reach the final equilibrium state, through a large amplitude C−Cl2 motion. Before this reactive state, the reactants are in a kind of "harmonic reversible" regime where each part still preserves its own electronic identity. What is new in our analysis is that the combination of time dependent ab initio calculations combined to different quantum chemical topology approaches well underlines this charge-transfer phenomenon and its amplitude as a driving force, revisiting and assessing, in a modern and accurate way, working hypotheses carried out in more approximate schemes.

5. Conclusion

In the present work, we have analyzed in some detail the bond formation mechanism for a prototype S_N2 reaction using static and dynamic approaches, both based on DFT and localized (Gaussian) basis sets. Combined with different QCT partitions of the molecular system in real space, we performed static and dynamic QCT analyses to examine intra- and intermolecular electronic charge transfers along the static reaction profile and the dynamic trajectory. Although our results exhibit similar global features in the static and dynamic approaches, only a dynamic QCT approach reveals the crucial role of the electron charge transfers during the formation of the ion−dipole complex, leading to spontaneous maximizations of covalent and noncovalent interactions.

Acknowledgment. The authors thank Prof. Zuccarello (Catania, Italy) for providing some reprints.

References

(1) Lewis, G. N. *J. Am. Chem. Soc.* **1916**, *38*, 762.

(2) Mulliken, R. S. *J. Chem. Phys.* **1955**, *23*, 1833.

(3) Löwdin, P. O. *J. Chem. Phys.* **1950**, *18*, 365.

(4) Del Re, G. *Theor. Chim. Acta* **1963**, *1*, 188.

(5) Pipek, J. P.; Mezey, G. *J. Chem. Phys.* **1989**, *90*, 4916.

(6) Reed, A. E.; Curtiss, L. A.; Weinhold, F. *Chem. Rev.* **1988**, 88, 899.

(7) Bader, R. F. W. *Atoms in Molecules: A Quantum Theory*; Oxford University Press: Oxford, England, 1990.

(8) Popelier, P. L. A. *Atoms in Molecules: An Introduction*; Pearson Education: London, England, 2000.

(9) Becke, A. D.; Edgecombe, K. E. *J. Chem. Phys.* **1990**, *92*, 5397.

(10) Silvi, B.; Savin, A. *Nature* **1994**, *371*, 683.

(11) Savin, A.; Silvi, B.; Colonna, F. *Can. J. Chem.* **1996**, *74*, 1088.

(12) Bader, R. F. W.; Johnson, S.; Tang, T. H.; Popelier, P. L. A. *J. Phys. Chem.* **1996**, *100*, 15398

(13) Fradera, X.; Austen, M. A.; Bader, R. F. W. *J. Phys. Chem. A* **1999**, *103*, 304.

(14) Cortés-Guzmán, F.; Bader, R. F. W. *Coord. Chem. Rev.* **2005**, *249*, 633.

(15) Merino, G.; Vela, A.; Heine, T. *Chem. Rev.* **2005**, *105*, 3812.

(16) Bader, R. F. W.; MacDougall, P. J. *J. Am. Chem. Soc.* **1985**, *107*, 6788.

(17) Chaudry, U. A.; Popelier, P. L. A. *J. Phys. Chem. A* **2003**, *107*, 4578.

(18) Berski, S.; Andrés, J.; Silvi, B.; Domingo, L. R. *J. Phys. Chem. A* **2003**, *107*, 6014.

(19) Michelini, M. D. C.; Russo, N.; Alikhani, M. E. *J. Comput. Chem.* **2005**, *26*, 1284.

(20) Santos, J. C.; Andrés, J.; Aizman, A.; Fuentealba, P.; Polo, V. *J. Phys. Chem. A* **2005**, *109*, 3687.

(21) Fukui, K. *Acc. Chem. Res.* **1981**, *14*, 363. Gonzalez, C.; Schlegel, H. B. *J. Chem. Phys.* **1989**, *90*, 2154.

(22) Solà, M.; Toro-Labbé, A. *J. Phys. Chem. A* **1999**, *103*, 8847.

(23) Polo, V.; Andrés, J. *J. Comput. Chem.* **2005**, *26*, 1427.

(24) Burns, T.; Marques, M. A. L.; Gross, E. K. U. *Phys. Rev. A* **2005**, *71*, 10501.

(25) Ziegler, T.; Autschbach, J. *Chem. Rev.* **2005**, *105*, 2695.

(26) Gleich, D.; Hutter, J. *Chem. Eur. J.* **2004**, *10*, 2435.

(27) Tateyama, Y.; Blumberger, J.; Sprik, M.; Tavernelli, I. *J. Chem. Phys.* **2005**, *122*, 234505.

(28) Car, R.; Parrinello, M. *Phys. Rev. Lett.* **1985**, *55*, 2471.

(29) Marx, D.; Hutter, J. In *Modern Methods and Algorithms of Quantum Chemistry Proceedings*; Grotendorst, J., Ed.; Forschungszentrum Jülich: NIC Series, 2000; Vol. 3, p 339.

(30) Ammal, S. C.; Yamataka, H.; Aida, M.; Dupuis, M. *Science* **2003**, *299*, 1555.

(31) Schlegel, H. B.; Millam, J. M.; Iyengar, S. S.; Voth, G. A.; Daniels, A. D.; Scuseria, G. E.; Frish, M. J. *J. Chem. Phys.* **2001**, *114*, 9758. Iyengar, S. S.; Shlegel, H. B.; Millam, J. M.; Voth, G. A.; Scuseria, G. E.; Frish, M. J. *J. Chem. Phys.* **2001**, *115*, 10291. Shlegel, H. B.; Iyengar, S. S.; Li, X.; Millam, J. M.; Voth, G. A.; Scuseria, G. E.; Frish, M. J. *J. Chem. Phys.* **2002**, *117*, 8694.

(32) Ho, W. P.; Truhlar, D. G. *J. Am. Chem. Soc.* **1995**, *117*, 10726.

(33) Gonzales, J. M.; Cox, R. S., III; Brown, S. T.; Allen, W. D.; Schaefer, H. F., III *J. Phys. Chem. A* **2001**, *105*, 11327.

(34) Ensing, B.; Meijer, E. J.; Blöchl, P. E.; Baerends, P. E. *J. Phys. Chem. A* **2001**, *105*, 3300.

(35) Cossi, M.; Adamo, C.; Barone, V. *Chem. Phys. Lett.* **1998**, *297*, 1.

(36) Adamo, C.; Barone, V. *J. Chem. Phys.* **1999**, *110*, 6158.

(37) Wladkowski, B. D.; Lim, K. F.; Allen, W. D.; Brauman, J. I. *J. Am. Chem. Soc.* **1992**, *114*, 9136 and references therein.

(38) Deng, L.; Branchadell, V.; Ziegler, T. *J. Am. Chem. Soc.* **1994**, *116*, 10645.

(39) Parthiban, S.; Oliveira, G. D.; Martin, J. M. L. *J. Phys. Chem. A* **2001**, *105*, 895.

(40) Yang, S.-Y.; Fleurat-Lessard, P.; Hristov, I.; Ziegler, T. *J. Phys. Chem A* **2004**, *108*, 9461.

(41) Streitwieser, A.; Choy, G. S.; Abu-Hasanayn, F. J. *J. Am. Chem. Soc.* **1997**, *110*, 5013.

(42) Sun, L.; Song, K., Hase, W. L. *Science* **2002**, *296*, 875.

(43) Schmatz, S.; Botschwina, P.; Hauschildt, J.; Schinke, R. *J. Chem. Phys.* **2001**, *114*, 5233.

(44) Botschwina, P. *Theor. Chem. Acc.* **1998**, *99*, 426.

(45) Gonzales, J. M.; Allen, W. D.; Schaefer, H. F. *J. Phys. Chem. A* **2005**, *109*, 10613.

(46) Bento, A. P.; Solà, M.; Bickelhaupt, F. M. *J. Comput. Chem.* **2005**, *26*, 1497.

(47) Lee, I.; Kim, C. K.; Soh, C. K.; Li, H. G.; Lee, H. W. *J. Phys. Chem. A* **2002**, *106*, 1081.

(48) Chandrasekhar, J.; Jorgensen, W. L. *J. Am. Chem. Soc.* **1985**, *107*, 2974.

(49) Gritsenko, O. V.; Ensing, B.; Schipper, P. R. T.; Baerends, E. J. *J. Phys. Chem. A* **2000**, *104*, 8558.

(50) Gonzales, J. M.; Cox, R. S.; Brown, S. T.; Allen, W. D.; Schaeffer, H. F. *J. Phys. Chem. A* **2001**, *105*, 11327.

(51) Barlow, S. E.; Van Doren, J. M.; Bierbaum, V. M. *J. Am. Chem. Soc.* **1988**, *110*, 7240.

(52) Larson, J. W.; McMahon, T. B. *J. Am. Chem. Soc.* **1985**, *107*, 766. Li, C.; Ross, P.; Szulejko, J. E.; McMahon, T. B. *J. Am. Chem. Soc.* **1996**, *118*, 9360. Wladkowski, B. D.; Brauman, J. I. *J. Phys. Chem.* **1993**, *97*, 13158.

(53) Frisch, M. J.; Trucks, G. W.; Schlegel, H. B.; Scuseria, G. E.; Robb, M. A.; Cheeseman, J. R.; Montgomery, J. A., Jr.; Vreven, T.; Kudin, K. N.; Burant, J. C.; Millam, J. M.; Iyengar, S. S.; Tomasi, J. Barone, V.; Mennucci, B.; Cossi, M.; Scalmani, G.; Rega, N.; Petersson, G. A.; Nakatsuji, H.; Hada, M.; Ehara, M.; Toyota, K.; Fukuda, R.; Hasegawa, J.; Ishida, M.; Nakajima, T.; Honda, Y.; Kitao, O.; Nakai, H.; Klene, M.; Li, S.; Knox, J. E.; Hratchian, H. P.; Cross, J. B.; Bakken, V.; Adamo, C.; Jaramillo, J.; Gomperts, R.; Stratmann, R. E.; Yazyev, O.; Austin, A. J.; Cammi, R.; Pomelli, C.; Ochterski, J. W.; Ayala, P. Y.; Morokuma, K.; Voth, G. A.; Salvador, P.; Dannenberg, J. J.; Zakrzewski, V. G.; Dapprich, S.; Daniels, A. D.; Strain, M. C.; Farkas, O.; Malick, D. K.; Rabuck, A. D.; Raghavachari, K.; Foresman, J. B.; Ortiz, J. V.; Cui, Q.; Baboul, A. G>; Clifford, S.; Cioslowski, J.; Stefanov, B. B.; Liu, G.; Liashenko, A.; Piskorz, P.; Komaromi, I.; Martin, R. L.; Fox, D. J.; Keith, T.; Al-Laham, M. A>; Peng, C. Y.; nanayakkara, A.; Challacombe, M.; Gill, P. M. W.; Johnson, B.; Chen, W.; Wong, M. W.; Gonzelez, C.; Pople, J. A. *Gaussian 03, Revision B.05*; Gaussian, Inc.: Wallingford, CT, 2004.

(54) Ernzerhof, M.; Scuseria, G. E. *J. Chem. Phys*. **1999**, *109*, 911

(55) Francl, M. M.; Petro, W. J.; Hehre, W. J.; Binkley, J. S.; Gordon, M.-H.; DeFree, D. J.; Pople, J. A. *J. Chem. Phys.* **1982**, *77*, 3654.

(56) Swope, W. C.; Andersen, H. C.; Berend, P. H.; Wilson, K. R. *J. Chem. Phys.* **1982**, *76*, 637.

(57) Silvi, B. *J. Phys. Chem. A* **2003**, *107*, 3081.

(58) Noury, S.; Krokidis, X.; Fuster, F.; Silvi, B. Topmod package, Université Pierre et Marie Curie, 1997.

(59) Soler, P.; Bergès, J.; Fuster, F.; Chevreau, H. *Chem. Phys. Lett.* **2005**, *411*, 117. Chevreau, H. *J. Chem. Phys.* **2005**, *122*, 244316.

(60) Popelier, P. L. A.; Aicken, F. M. *Chem. Phys. Chem.* **2003**, *4*, 824.

(61) Toulouse, J.; Savin, A.; Adamo, C. *J. Chem. Phys*. **2002**, *117*, 10465.

(62) Blavins, J. J.; Cooper, D. L.; Karadakov, P. B. *J. Phys. Chem. A* **2004**, *914*, 108.

(63) Cioslowski, J.; Karkowski, J. *Quantum-Mechanical Theory of Atoms in Molecules: A Relativistic Formulation in Fundamentals of Molecular Similarity*; Kluwer Academic: 2001; p 101

(64) Cioslowski, J.; Mixon, S. T. *Can. J. Chem.* **1992**, *70*, 443.

(65) Cioslowski, J.; Mixon, S. T. *J. Am. Chem. Soc.* **1992**, *114*, 4382.

(66) Feinberg, M. J.; Ruedenberg, K. *J. Chem. Phys*. **1971**, *54*, 1495

(67) Shaik, S. S. *J. Am. Chem. Soc.* **1981**, *103*, 3692

(68) Rastelli, A.; Bozzoli, A. S.; Del Re, G. *J. Chem. Soc., Perkin Trans 2* **1972**, 1571

(69) Zuccarello, F.; Del Re, G. *J. Comput. Chem.* **1987**, *6*, 816.

(70) Toro-Labbé, A. *J. Phys. Chem.* **1999**, *103*, 4398.

CT0600159